Scaling study of dynamical smeared-link clover fermions

S. Dürr,[1] Z. Fodor,[1,2,3] C. Hoelbling,[2] R. Hoffmann,[2] S. D. Katz,[2,3] S. Krieg,[4] T. Kurth,[2] L. Lellouch,[5] T. Lippert,[1,2,4] K. K. Szabo,[2] and G. Vulvert[5]

(Budapest-Marseille-Wuppertal Collaboration)

[1]*NIC, DESY Zeuthen, D-15738 Zeuthen and FZ Jülich, D-52425 Jülich, Germany*
[2]*Bergische Universität Wuppertal, Gaussstr.20, D-42119 Wuppertal, Germany*
[3]*Institute for Theoretical Physics, Eötvös University, H-1117 Budapest, Hungary*
[4]*Jülich Supercomputing Center, FZ Jülich, D-52425 Jülich, Germany*
[5]*Centre de Physique Théorique*, Case 907, Campus de Luminy, F-13288 Marseille Cedex 9, France*
(Received 27 March 2008; published 5 January 2009)

We present a framework for phenomenological lattice QCD calculations which makes use of a tree-level Symanzink improved action for gluons and stout-link Wilson fermions. We give details of our efficient HMC/RHMC algorithm and present a scaling study of the low-lying $N_f = 3$ baryon spectrum. We find a scaling region that extends to $a \lesssim 0.16$ fm and conclude that our action and algorithm are suitable for large scale phenomenological investigations of $N_f = 2 + 1$ QCD. We expect this conclusion to hold for other comparable actions.

I. INTRODUCTION

Over the last decade, it has become clear that smeared-link fermion actions[1] offer substantial technical advantages over their thin-link counterparts. The idea of damping unphysical UV fluctuations by replacing elementary links with a weighted sum of paths was first introduced in the framework of pure gauge theory [1]. It was later recognized that the chiral properties of clover fermions [2] can be substantially improved by replacing the thin links in the covariant derivative of the fermion operator with their smeared counterparts [3]. From a Symanzik point of view, this replacement amounts to adding ultralocal irrelevant terms to the fermion action, as long as the smearing prescription (parameter, iteration number) stays fixed as a function of bare coupling. In this way it is guaranteed that the continuum limit is unchanged.

In the context of quenched QCD, the advantages of smeared clover fermions are well established [3–8]. The theoretically leading $O(\alpha_s a)$ contributions are, in practice, absent and the extrapolation to the continuum appears to be dominated by $O(a^2)$ cutoff effects. In particular, the tamed UV fluctuations result in improved chiral symmetry properties. Furthermore, the smearing significantly reduces the contributions of unphysical tadpoles; renormalization constants are generally closer to their tree-level values, and $c_{\rm SW}$ is not far from 1 at typical lattice spacings.

Given this experience, it is reasonable to expect that also dynamical clover fermions will benefit from link smearing. There, the nondifferentiable nature of the back projection step of the smeared link onto the gauge group, which is usually performed, for instance, when using APE smearing [1], may pose problems for the molecular dynamics update. An early suggestion was to use "stout" links [9] to define fermions which can be simulated with the hybrid Monte Carlo (HMC) algorithm [10]. Further particulars of the HMC force with UV-filtered actions have been worked out in [11]. Recently, several alternative smearing methods suitable for dynamical simulations have been proposed [8,12–16].

The efficiency of link smearing results from the fact that it leaves the structure of the fermionic operator entirely unchanged. Smeared clover fermions still have exclusively nearest-neighbor couplings. The damping of unphysical UV modes is achieved exclusively by a modified—but still ultralocal—coupling to the gluonic background. This modification of the fermionic action is continuum irrelevant, but at a given finite cutoff one generally expects observables with weaker coupling to unphysical UV modes to be closer to their continuum limit values, resulting in overall improved scaling. In the present paper we investigate this issue by performing a scaling study with $N_f = 3$, stout-link clover fermions. Although other smearing methods are presently known, we opt for the standard stout-link prescription because it is widely used and will share features, such as an enlarged scaling region, with other comparable prescriptions.

The size of its scaling region is one of the most important criteria to assess the suitability of a given action for phenomenological purposes. The onset of scaling, together with the power of the lattice spacing against which results

---

*CPT is "UMR 6207 du CNRS et des universités d'Aix-Marseille I, d'Aix-Marseille II et du Sud Toulon-Var, affiliée à la FRUMAM".

[1]In the literature they are also referred to as "UV-filtered" or "fat-link" actions. Likewise, actions in which the covariant derivative involves the original gauge links are sometimes called "thin-link" actions.

need to be plotted to show a linear dependence, determines the finest lattice spacing needed to reliably extrapolate to the continuum, and hence the overall cost in terms of CPU time. Our main result is that smeared clover fermions do indeed show very nice scaling properties up to at least 0.16 fm lattice spacing. Moreover, the link-smearing seems to eliminate known pathologies that unfiltered actions may show in a dynamical setting [17,18].

The results presented in this paper are obtained using a tree-level Symanzik improved gauge action [19] and six-step, stout-smeared clover fermions with a clover coefficient taken at its tree-level value $c_{SW} = 1$ (though a perturbative [20,21] or nonperturbative [15,22] determination is feasible). Note that also $F_{\mu\nu}$ in the clover term is built from the same set of stout links. This choice allows for efficient simulation while delivering good scaling properties, as demonstrated below. Moreover, dedicated studies in quenched QCD have shown that the dependence of observables on smearing is quite mild (see e.g. [8,13]) and the exploratory studies of e.g. [11,12,14–16] suggest that this behavior persists in the full theory. Thus, our choice involves no fine-tuning and we expect our results to hold for actions which involve comparable amounts of smearing.

In our scaling study we choose $N_f = 3$ for simplicity, creating an artificial world with degenerate u, d and s quarks. We will denote the pseudoscalar and vector mesons by π and ρ respectively. Our goal is to perform continuum extrapolations along three distinct lines of constant "physical" quark masses, characterized by $M_\pi/M_\rho = 0.60, 0.64,$ and 0.68. Since we do not aim in this paper at phenomenologically relevant computations and instead would like to test the extent of the scaling regime, we deliberately choose these rather large masses. With Ma for standard hadrons close to 1, cutoff effects with inferior actions will be large. In all our runs $M_\pi L$ is kept fixed, at values larger than 4, to avoid finite-volume effects. Our goal is to simulate at several values of the gauge coupling and fixed M_π/M_ρ and $M_\pi L$, and to determine the scaling of the baryon octet and decuplet masses, M_N and M_Δ.

The remainder of the article is organized as follows. In Sec. II details of the action and our algorithm are given. Sections III and IV are devoted to tests which provide clear evidence for the absence of bulk phase transitions in our simulations. In Sec. V we show that our action is ergodic with respect to topology. Section VI then contains a detailed scaling study of the nucleon and delta masses. We conclude with a short summary and outlook.

II. ACTION AND ALGORITHMS

A. Action

The explicit form of our gauge and fermion action in terms of the thin ($U_{n,\mu}$) and smeared ($V_{n,\mu}$) gauge links is as follows:

$$S = S_G^{Sym} + S_F^{SW}$$

$$S_G^{Sym} = \beta\left[\frac{c_0}{3}\sum_{plaq} Re\, Tr(1 - U_{plaq})\right.$$

$$\left. + \frac{c_1}{3}\sum_{rect} Re\, Tr(1 - U_{rect})\right] \quad (1)$$

$$S_F^{SW} = S_F^{W}[V] - \frac{c_{SW}}{4}\sum_{n}\sum_{\mu,\nu}\bar{\psi}_x\sigma_{\mu\nu}F_{\mu\nu,n}[V]\psi_x,$$

with the standard Wilson action S_F^W. The parameters c_{SW}, c_0 and c_1 set to their tree-level values:

$$c_{SW} = 1, \qquad c_1 = -1/12, \qquad c_0 = 1 - 8c_1 = 5/3.$$

Both the hopping part and the clover improvement term in the fermion action S_F^{SW} use six-step stout-smeared links [9] $V_{n,\mu} \equiv V_{n,\mu}^{(6)}$. Those are constructed from the thin links $U_{n,\mu} \equiv V_{n,\mu}^{(0)}$ according to

$$V^{(n+1)} = e^{\rho S^{(n)}}U^{(n)},$$

$$S^{(n)} = \tfrac{1}{2}(\Gamma^{(n)}V^{(n)\dagger} - V^{(n)}\Gamma^{(n)\dagger}) - \tfrac{1}{6}Re\, Tr(\Gamma^{(n)}V^{(n)\dagger}$$
$$- V^{(n)}\Gamma^{(n)\dagger}) \quad (2)$$

$$\Gamma_{n,\mu}^{(n)} = \sum_{\nu\neq\mu}V_{n,\nu}^{(n)}V_{n+\nu,\mu}^{(n)}V_{n+\mu,\nu}^{(n)\dagger}$$

The stout smearing parameter is chosen to be $\rho = 0.11$, which is a rather conservative choice [8,9] corresponding to an $\alpha_{APE} = 0.48$ with respect to the average plaquette [12]. In S_G^{Sym} only the unfiltered links are used. As detailed in the Introduction, this action is ultralocal in both the quark and gauge sector.

B. Simulation algorithm

We start with the description of our $N_f = 2 + 1$ algorithm. Two flavors are implemented via the HMC algorithm [10], the third using the rational hybrid Monte Carlo (RHMC) algorithm [23,24]. We employ even/odd preconditioning [25] to speed up the fermion matrix inversions. The generic HMC algorithm suffers from critical slowing down in the light-quark regime. To treat this problem, we combine several improvements over the generic algorithm (see also [26,27]):

(i) *Multiple time-scale integration:* not all force contributions in the molecular dynamics (MD) part of the HMC algorithm require the same amount of computational resources. Using multiple time-scale integration ("Sexton-Weingarten integration scheme") [28], it is possible to put each part of the MD on a different time scale according to its relative contribution to the total force, thus reducing the computational costs of the MD.

(ii) *Mass preconditioning:* the pseudofermion force is used within the MD to include the effects of dynamical fermions. Through mass preconditioning, the UV

part of the force can be split off and treated separately [29], which helps reducing the fluctuations in the force. The second important benefit of mass preconditioning appears when combined with the multiple time-scale integration scheme [26,27]: the more expensive infrared part contributes less to the total force and can be integrated with larger time steps.

(iii) *RHMC:* the third, unpaired quark flavor is implemented through the RHMC [23,24] algorithm. This algorithm makes use of the fact that the single fermion action can be written as $\xi^\dagger (M^\dagger M)^{-1/2}\xi$, where the inverse square root can in turn be approximated by a rational approximation and be efficiently calculated with a multishift solver. The RHMC is highly efficient in simulating a single quark flavor. It can also be combined with the multiple time-scale integration scheme.

(iv) *Omelyan integrator:* the MD integration within the generic HMC algorithms uses the leapfrog integration scheme. It proceeds by first integrating one half step in position space followed by a full step update of the conjugate momenta and finally another half step in position space. The Omelyan integrator adds a small momentum update (reduced by $\lambda \approx 0.193$) before and after the leapfrog step and shortens the original leapfrog momentum update in by a factor $(1–2\lambda)$. This scheme improves the MD energy conservation by about 1 order of magnitude for a factor ~ 2 increase in computational cost. The use of a correspondingly larger step size then results in a net gain of about 50% [30].

We use this algorithm also for our $N_f = 3$ scaling study with $m_{\mathrm{HMC}} = m_{\mathrm{RHMC}}$.

C. Inversion algorithms

The most time consuming part, both in the valence and the sea sector, is the (approximate) fermion matrix inversion by means of a linear solver. These calculations generally require double precision accuracy. This is due to the fact that, in order to maintain reversibility, the MD part of the algorithm has to be performed in double precision. Double precision accuracy is also required in valence calculations at small quark masses, owing to the large condition numbers involved. However, this does not imply that each fermion matrix multiplication needs to be done in double precision. In the valence sector we need to solve

$$Dx = b \qquad (3)$$

(with D in our case being the stout-link clover Dirac operator) to construct the correlators. To calculate the fermionic force in the MD part of the algorithm we need to solve

$$D^\dagger D x = b. \qquad (4)$$

In both cases it is possible to use a single precision version of D within mixed precision solvers to accelerate the inversion. There is basically no penalty in terms of the iteration count: we find that the increase in the number of matrix multiplications is well below 10%.

A simple and reasonably efficient way to construct a mixed precision solver is to use the standard "iterative refinement" technique, which amounts to repeatedly using a single precision solver. In this scheme, only the (outer) residuals and global sums are calculated in double precision; the inversion is performed with single precision accuracy. The single precision inversion typically uses the same algorithm that would be used for a full double precision inversion, such as BiCGstab to solve (3) or CG for (4). With $\mathbf{A} = D$ or $\mathbf{A} = D^\dagger D$ referring to the forward multiplication routine in double precision, $\mathbf{a}$ the single precision counterpart and ϵ the desired final double precision accuracy, the complete procedure reads:

(1) Compute $r_i = b - \mathbf{A}x_i$
(2) If $|r_i| \le \epsilon |b|$, exit
(3) Solve $\mathbf{a}t_i = r_i$ in single precision to an accuracy ϵ', with $\tilde{t}_i$ denoting the solution.
(4) Update $x_{i+1} = x_i + \tilde{t}_i$
(5) Goto 1

With $s_i = r_i - \mathbf{A}\tilde{t}_i$ and $\delta \equiv |s_i|/|r_i| \approx \epsilon' < 1$, we have

$$|r_{i+1}| = |b - \mathbf{A}x_{i+1}| = |b - \mathbf{A}x_i - \mathbf{A}\tilde{t}_i|$$
$$= |b - \mathbf{A}x_i - r_i + s_i| = |s_i| = \delta|r_i| < |r_i|. \quad (5)$$

Thus, as long as the single precision inversion does not fail, the method will converge. Since many single precision matrix multiplications are needed to compute $\tilde{t}_i$, compared to just one double precision multiplication with $\mathbf{A}$ in the outer iteration, the whole solver is dominated by the single
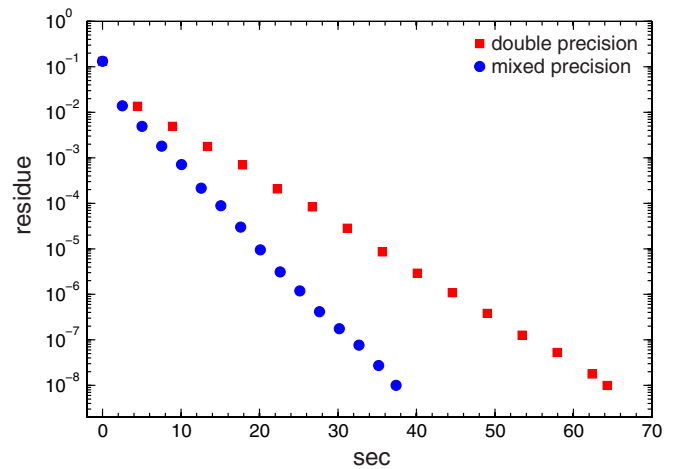

FIG. 1 (color online). Performance of CG in double precision (squares) compared to a mixed precision variant of CG (circles). Data are from an $N_f = 2 + 1$ run on a $32^3 \times 64$ lattice at $\beta = 3.57$ with $am_{ud}^{\mathrm{PCAC}} \simeq 0.0077$ and $am_s^{\mathrm{PCAC}} \simeq 0.049$ corresponding to $M_\pi \sim 250$ MeV.

precision matrix multiplication performance, resulting in a significant speedup over a full double precision inversion (see Fig. 1).

II. SPECTRAL GAP

In quenched QCD, the (unsmeared) clover fermion operator may have one or several eigenvalues close to the origin or with a negative real part, even for not very light quark masses. Configurations for which this is the case are referred to as "exceptional."

If one integrated the HMC trajectories exactly, any such configuration would be absent in full QCD, since an eigenvalue of the hermitean Wilson operator $H_W = \gamma_5 D_W$ approaching zero would induce an infinite back-driving force in the HMC. In practice, when the trajectories are generated with a finite step-size integrator, the near zero modes along a trajectory are only approximately suppressed. This may cause a breakdown of the MD evolution. It is therefore natural to monitor the smallest eigenvalue (in magnitude) of H_W and check if it is sufficiently far from the origin throughout the entire run. In a given ensemble this spectral gap shows a more-or-less Gaussian distribution, and as long as its median is several σ away from zero, the simulation is deemed safe [31].

Since we use even-odd preconditioning, the relevant quantity to monitor is the smallest eigenvalue of the Hermitian counterpart of the reduced operator $D_{\rm red} = \frac{1}{2} \times (D_{\rm oo} - D_{\rm oe} D_{\rm ee}^{-1} D_{\rm eo})$, which is γ_5-Hermitian. We include a factor $1/2$ to have its IR eigenvalues almost aligned with the low-lying eigenvalues of the full operator. For the lightest mass ($M_\pi/M_\rho = 0.60$, cf. Sec. V) the distributions are shown in Fig. 2, with β ranging from 2.8 (left) to 3.76 (right). One can see that even for the strongest coupling, there is still a clear separation of the eigenmodes from the origin.

For phenomenological applications it is of course most relevant to know how this spectral gap evolves when lowering the masses of two of the three flavors. Instead of monitoring the lowest eigenvalue of $\gamma_5 D_{\rm red}$, we opted for monitoring the closely related quantity $1/n_{\rm CG}$, where $n_{\rm CG}$

FIG. 3 (color online).   Histogram of the inverse iteration number of our linear solver at a lighter M_π for the lightest pseudo-fermion in the action. Results are from an $N_f = 2 + 1$ run on a $48^3 \times 64$ lattice at $\beta = 3.57$ with $am_{ud}^{\rm PCAC} \simeq 0.0056$ and $am_s^{\rm PCAC} \simeq 0.044$ corresponding to $M_\pi \sim 190$ MeV.

is the iteration count for the lightest pseudofermion in the action for our $N_f = 2 + 1$ runs. In Fig. 3, we plot a histogram of $1/n_{\rm CG}$ for one of our lightest production runs (for phenomenological studies) and find a clear gap, which provides strong evidence for the stability of the algorithm. We have also monitored the acceptance rate and the Hamiltonian violation ΔH throughout our runs and have seen no sign of any algorithmic problems.

IV. SEARCH FOR POTENTIALLY METASTABLE BEHAVIOR

In dynamical Wilson fermion simulations with small quark masses, it was reported that the system appears to undergo a first-order transition to an unphysical phase [18,32]. This was argued to mean that there is a lower bound on the quark mass, below which physically sensible simulations cannot be performed. Moreover, it was observed, that
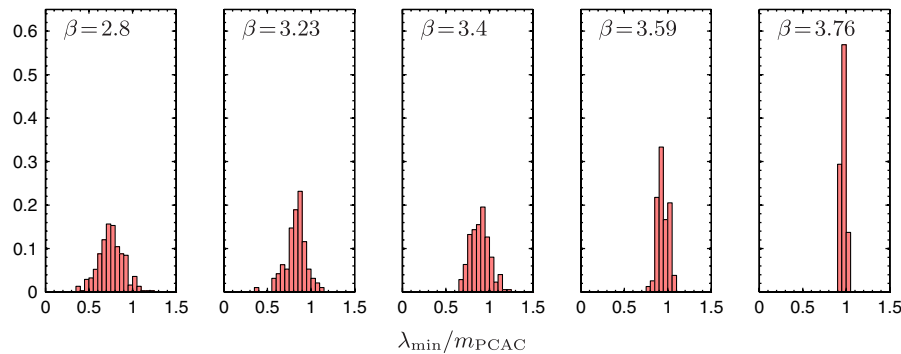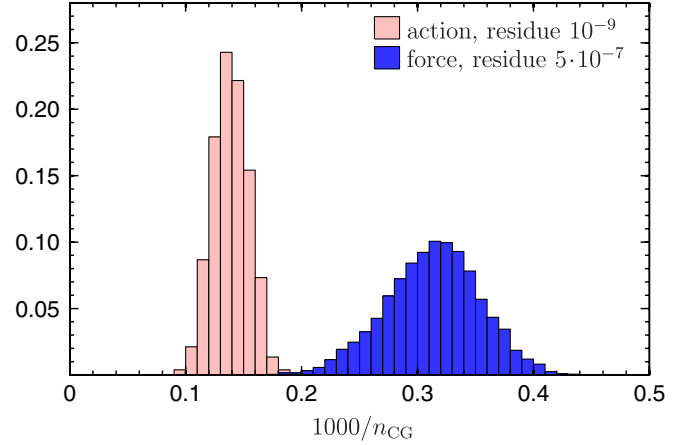
(1) the phenomenon occurs only with coarse lattices,

FIG. 2 (color online).   The magnitude of the smallest eigenvalue of the preconditioned Hermitian Dirac operator in units of the PCAC mass. At each β the lightest run ($M_\pi/M_\rho \simeq 0.6$) is shown.

(2) gauge action improvement decreases the lower bound on the quark mass [33],

(3) $O(a)$-improved Wilson fermions together with improved gauge actions made the problem disappear for all lattice spacings investigated in [18],

(4) one level of stout smearing weakens the phenomenon [34].

When discussing such phenomena, it is important to remember that a first-order phase transition can only occur in infinite volume. In finite volume, the metastability can be understood as an artifact of the updating algorithm: with an efficient algorithm, the system should eventually find the true minimum of the effective potential. Thus, for finite-volume simulations, the relevant question is: can the algorithm thermalize the system in a manageable number of updating steps?

To investigate this issue, we have taken two $16^3 \times 32$ configurations, one with random links and the other, thermalized in a $N_f = 2 + 1$ simulation at $\beta = 3.3$, with $am_{u,d}^{\mathrm{PCAC}} = 0.0066$, corresponding to a pion mass of approximately 240 MeV, and $am_s^{\mathrm{PCAC}} \simeq 0.0677$, corresponding roughly to the physical strange quark mass. A "downward" updating sequence was then constructed from the random configuration: consecutive simulations at $am_{u,d}^{\mathrm{PCAC}} \simeq 0.0243, 0.0173, 0.0131, 0.0086, 0.0066$, corresponding to a range of pseudoscalar masses $M_\pi \sim 440 - 240$ MeV, were performed, with each simulation starting from the last configuration of the previous (larger mass) run. Similarly, an "upward" sequence of five simulations was obtained, beginning with the configuration thermalized at $am_{u,d}^{\mathrm{PCAC}} \simeq 0.0066$, and ending with a run at $am_{u,d}^{\mathrm{PCAC}} \simeq 0.0243$. For each point in the two sequences,

approximately 400 trajectories were generated, of which the first 100 were discarded when calculating the average expectation value of the plaquette. The resulting plaquette values, obtained during the two updating sequences, are shown in Fig. 4. No sign of hysteresis is observed: the algorithm evolves the system to the correct equilibrium state in a reasonable number of steps, independently of the starting configuration.

This absence of evidence for metastability, together with the good performance of our algorithm in all of our production runs, gives us confidence that our choice of algorithm and of action is appropriate for the range of parameters that we have considered so far.

V. TOPOLOGY

In phenomenological applications, the combined choice of an action and an algorithm must allow for an adequate sampling of sectors of different topological charge. Quite generically, this sampling becomes more difficult as the
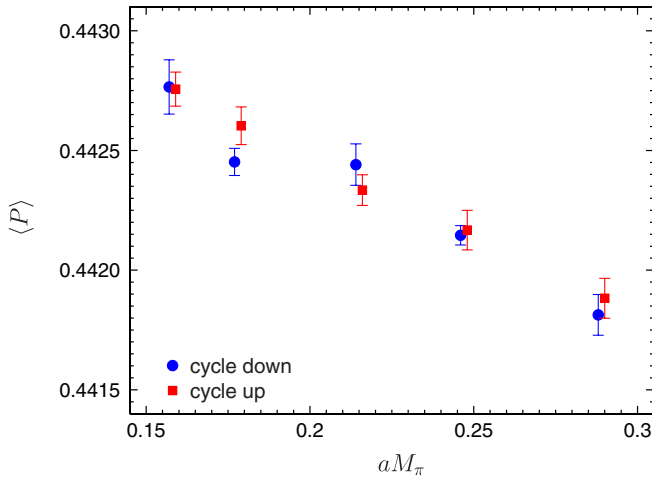

FIG. 4 (color online). Absence of hysteresis in the average expectation value of the plaquette. Data are from an $N_f = 2 + 1$ run on a $16^3 \times 32$ lattice at $\beta = 3.3$ with a fixed strange quark mass $am_s^{\mathrm{PCAC}} \simeq 0.0677$ and the light quark mass varying between $am_{ud}^{\mathrm{PCAC}} \simeq 0.0066$ and 0.0243 in ascending (square) and descending (circles) order. The range of light quark masses corresponds to $M_\pi \sim 240$–440 MeV. The second data set is slightly offset along the x-axis for better readability.
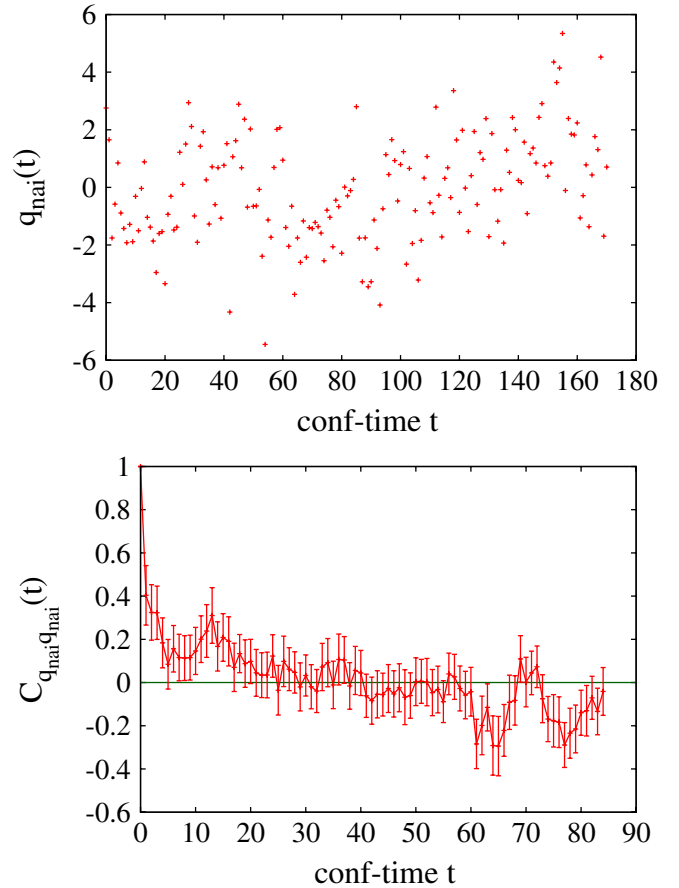

FIG. 5 (color online). History of the unrenormalized gluonic topological charge (left) and the corresponding autocorrelation function plot (right), measured on our finest lattice with the smallest quark mass: $\beta = 3.76$, $aM_\pi = 0.2019(20)$. The integrated autocorrelation time of q_{nai} is approximately 2 configurations on this ensemble. A separation of one configuration corresponds to 10 HMC/RHMC trajectories.

continuum limit is approached. Thus, as the lattice spacing is reduced, the autocorrelation time of topological charge increases. This is also the case in our simulations. However, within the range of lattice spacings which we consider, we observe no dramatic slowing down of tunneling events.

To determine the topological charge of our configurations, we use the naive gluonic charge definition

$$q_{\text{nai}} = \frac{1}{16\pi^2} \sum_x \text{Tr}[F_{\mu\nu}(x)\tilde{F}^{\mu\nu}(x)], \qquad (6)$$

where $F_{\mu\nu}$ is the gluonic field strength tensor and the sum extends over all lattice sites. We calculate $F_{\mu\nu}$ at each lattice site as follows. After applying our smearing prescription (2) to the links, we average the four plaquettes emanating from this site and which lie in the μ-ν plane. The field strength tensor is then defined as the anti-Hermitian part of this average. The charge defined in Eq. (6) leads to noninteger values and must be renormalized for quantitative studies of topology. However, such a renormalization is not necessary here since we are only interested in verifying the topological ergodicity of our simulations.

The simulation-time evolution and autocorrelation of this unrenormalized topological charge are shown in Fig. 5 for our finest lattice and its smallest quark mass, $aM_\pi = 0.2019(20)$. The integrated autocorrelation time is around 2 configurations. The autocorrelation decays very rapidly and is compatible with zero within the error bars

after around 5 configurations. We can easily conclude from these two plots that there is no long-range correlation.
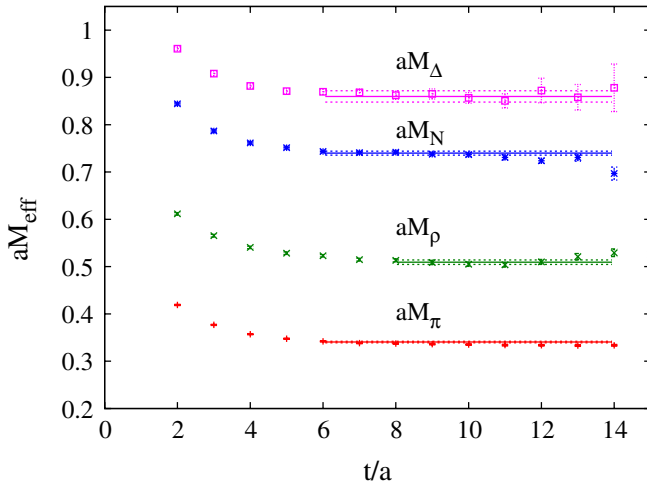

FIG. 6 (color online).   Effective masses of the pion, rho, nucleon and delta on our ensemble with $L/a = 16$, $\beta = 3.59$, $am_{\text{PCAC}} = 0.046\,08(12)$. The points are obtained by solving, for aM_{eff}, the equation $C(t-1)/C(t+1) = f(aM_{\text{eff}}(t-1-T/2))/f(aM_{\text{eff}}(t+1-T/2))$ at each t, where $f(x) = \cosh(x)$ (for π and ρ) or $f(x) = \sinh(x)$ (for N and Δ). The horizontal lines are the masses with error bars obtained from correlated cosh or sinh fits to the corresponding two-point functions in the time intervals indicated by the length of the lines.
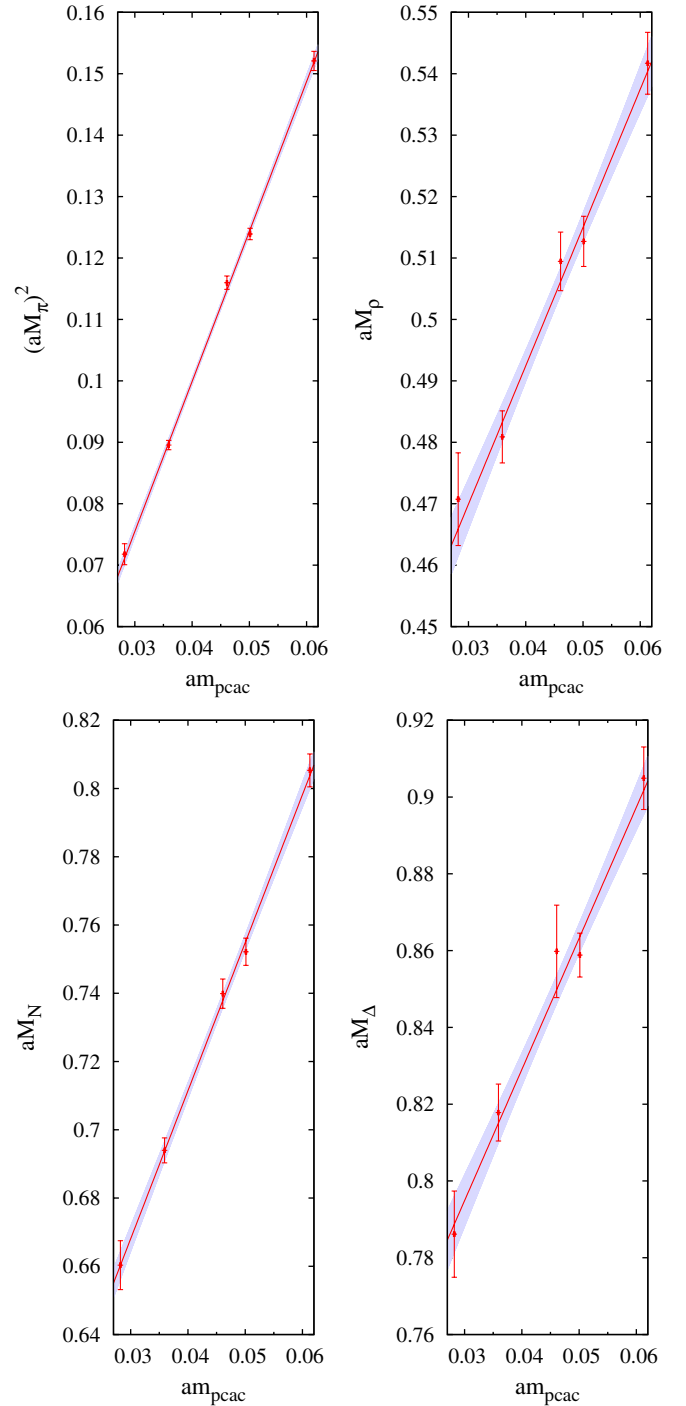

FIG. 7 (color online).   Linear fits of the spectrum in terms of the PCAC quark mass. Data shown are from $\beta = 3.59$, $L/a = 16$ simulations. The line indicates the central value of the interpolation and the shaded region is the corresponding 1σ error band (based on the assumption that the linear ansatz is correct).

VI. SCALING STUDY

For our scaling study, we use lattices with approximately constant physical volume at five different lattice spacings. We opted for an $N_f = 3$ instead of an $N_f = 2$ setting in order to test the full RHMC algorithm that is also being used for phenomenological applications. We choose a $T = 2L$ geometry with lattice sizes varying from $L/a = 8$ to $L/a = 24$ and bare gauge couplings between $\beta = 2.8$ and $\beta = 3.76$. We measure fermionic observables every 20 trajectories for $L/a = 8$, 10, 12 and every ten for $L/a = 16$, 24. For the error analysis, we use the "moving-block-bootstrap" [35] technique with a bin length of 2 times the integrated autocorrelation time of the quantity which is measured. This bin length is typically around 2 for the coarsest lattices and around 8 for the finest lattices. The number of bootstrap samples is chosen to be 2000, because the calculated bootstrap errors saturate at $\simeq 1500$ samples.

At each lattice spacing we simulate a number of masses (from seven at $L/a = 8$ to three at $L/a = 24$) such that M_π/M_ρ is between 0.60 and 0.68. As already mentioned in the Introduction, it is preferable to use these rather large masses for a scaling study in order to enhance possible discretization effects of order Ma. After fixing to Coulomb gauge, we measure propagators with multiple Gaussian sources on different time slices. The source size is set to $L/4$ and is thus roughly constant in physical units. Using a Gaussian sink of the same size, the effective masses usually reach a plateau very quickly and we can determine a useful fitting window from it. Note that—because the x-space (ultra-)locality of our action is the same as for the unsmeared clover action—such a "normal" behavior is exactly what one would expect. To illustrate this point, a typical effective mass plot is shown in Fig. 6. Then, the masses are extracted from a correlated single channel cosh

or sinh fit to the correlators. In order to estimate the systematic error due to excited states, we reduced the initial fit time by up to 2 time slices and repeated the analysis with the new fit ranges. This difference then propagates into the systematic error in the continuum limit.

For each coupling β we then interpolate $a^2 M_\pi^2$, aM_ρ, aM_N, and aM_Δ linearly to a common current quark mass as determined by M_π/M_ρ. For illustration the interpolation at $\beta = 3.59$ is shown in Fig. 7. The error on the current quark mass is of order 10^{-4} and therefore barely visible on this scale. Note that all data points are fully unquenched.

We perform our scaling test on the baryon spectrum for three different values of M_π/M_ρ, all of which can be reached by interpolating our simulation data. In Table I we summarize the values of am_{PCAC}, aM_π, aM_ρ, aM_N, and aM_Δ after interpolation to $M_\pi/M_\rho = 0.60$, 0.64, 0.68. Also listed is LM_π, which is roughly constant for fixed M_π/M_ρ. Moreover, even for the lightest data set we are deep in the $M_\pi L > 4$ regime. In case this criterion alone would not guarantee the smallness of finite-volume effects, the fact that our boxes have a fixed physical size ensures that such effects would be the same for all data at a given M_π/M_ρ ratio, and the scaling test would still be meaningful.

The masses are known to better than 2% and, due to correlations, this is also true for mass ratios. For the three lines of constant physics, M_N and M_Δ in units of M_π are plotted in Fig. 8 as functions of the squared lattice spacing (see below), measured in units of the vector meson mass. We normalize the baryon masses by M_π to clearly separate the lines of constant physics in the plot. The fits incorporate the error bars along both the vertical and horizontal axes.

For both the spin-1/2 and spin-3/2 baryons, the continuum limit is approached smoothly with scaling violations

TABLE I. Results of the interpolation of aM_π, aM_ρ, aM_N, and aM_Δ, obtained from simulations performed at different bare quark masses and gauge couplings, to the reference points $M_\pi/M_\rho = 0.60$, 0.64, 0.68.

M_π/M_ρ	L/a	β	am_{PCAC}	LM_π	aM_π	aM_ρ	aM_N	aM_Δ
0.60	8	2.80	0.0676(11)	4.55	0.5688(26)	0.9480(44)	1.3605(73)	1.5944(75)
	10	3.23	0.0468(28)	4.44	0.4437(57)	0.7395(95)	1.064(12)	1.248(10)
	12	3.40	0.0437(15)	4.60	0.3830(34)	0.6384(57)	0.9236(74)	1.0823(87)
	16	3.59	0.0328(6)	4.56	0.2852(26)	0.4754(43)	0.6785(44)	0.8031(38)
	24	3.76	0.0217(7)	4.85	0.2019(20)	0.3365(33)	0.4825(34)	0.5708(20)
0.64	8	2.80	0.0839(8)	5.03	0.6292(21)	0.9832(33)	1.4341(43)	1.6581(59)
	10	3.23	0.0607(23)	4.95	0.4950(47)	0.7735(73)	1.127(10)	1.3074(82)
	12	3.40	0.0545(13)	5.12	0.4268(23)	0.6669(35)	0.9711(62)	1.1282(71)
	16	3.59	0.0405(6)	5.03	0.3146(23)	0.4916(36)	0.7099(35)	0.8278(28)
	24	3.76	0.0270(6)	5.41	0.2256(18)	0.3524(28)	0.5081(29)	0.5933(29)
0.68	8	2.80	0.1050(11)	5.60	0.6993(22)	1.0284(32)	1.5286(52)	1.7401(65)
	10	3.23	0.0796(21)	5.57	0.5574(52)	0.8198(76)	1.212(11)	1.389(10)
	12	3.40	0.0693(12)	5.76	0.4798(30)	0.7055(44)	1.0354(47)	1.1903(52)
	16	3.59	0.0506(7)	5.57	0.3483(22)	0.5122(32)	0.7495(30)	0.8590(41)
	24	3.76	0.0343(9)	6.11	0.2546(25)	0.3744(37)	0.5434(38)	0.6242(39)

FIG. 9 (color online). Scaling of the Δ and nucleon mass at $M_\pi/M_\rho = 0.67$ in physical units using the scale setting procedure described around (7). In the continuum we obtain $M_N = 1490(7)(27)$ MeV and $M_\Delta = 1720(10)(35)$ MeV. As in Fig. 8, only statistical errors are shown.

For illustrative purposes, we set the scale by linearly interpolating M_ρ and M_π^2 to the point where

$$M_\pi/M_\rho = \sqrt{2(M_K^{\text{phys}})^2 - (M_\pi^{\text{phys}})^2}/M_\phi^{\text{phys}} \sim 0.67 \quad (7)$$

and identify M_ρ with the mass of the physical ϕ. In this convention we cover lattice spacings from about 0.19 down to 0.07 fm (see Fig. 9). In this range we find only small scaling violations in the spectrum and those disappear smoothly toward the continuum. The behavior is consistent with that of an O(a)-improved theory.

The scaling of other observables, especially matrix elements, will be investigated in the future.

VII. SUMMARY

We have described an efficient algorithm to perform full lattice QCD calculations with stout-link, improved clover fermions and demonstrated its potential with a scaling study of light baryon masses in $N_f = 3$ QCD. We have tested the algorithm and found it to be stable and reliable down to relatively coarse lattices with $a \simeq 0.16$ fm. We have also monitored the stability of the MD integration and the lowest eigenvalue of the (even-odd preconditioned) fermion matrix and demonstrated that the latter is sufficiently far away from zero on all of our ensembles. Furthermore, we have shown that there is no sign of exceptional configurations even with substantially lighter pion masses in an $N_f = 2 + 1$ setting.

Upon performing a ''thermal cycle'' at $\beta = 3.3$, with M_π ranging between ~240 MeV and ~440 MeV, we do not see any sign of a hysteresis. In other words, there is no indication of a nearby first-order phase transition, even on fairly coarse lattices and for rather light quark masses.

FIG. 8 (color online). M_N and M_Δ, the mass of the spin-1/2 and spin-3/2 baryon, in terms of M_π, versus the lattice spacing squared (in terms of M_ρ^{-1}). Each one of the three continuum extrapolations is based on the data at $\beta = 3.76 - 3.23$, but the curve is extended to $\beta = 2.8$ to allow for comparison. The continuum limits are $M_N/M_\pi = 2.378(17)(43)$, $2.245(10)(51)$, $2.127(7)(34)$ and $M_\Delta/M_\pi = 2.827(23)(40)$, $2.626(17)(49)$, $2.446(16)(30)$, respectively. For all data points only statistical errors are shown.

of at most 1.2% at $\beta = 2.8$. The extrapolations shown exclude this data point but consistent results are obtained by using all available data.

While we expect that our choice of the clover coefficient is close to a nonperturbatively determined value, we cannot exclude effects that are linear in the lattice spacing in principle. The cutoff effects that we consider here are so small that we cannot make a definitive statement, despite the fact that we have very precise data and cover more than a factor of 7 in a^2. Assuming the lattice artifacts to be linear in a results in an only marginally worse fit.

An alternative way of proceeding is doing a combined chiral and continuum extrapolation with all data points at once. Applying this procedure one obtains basically consistent continuum limits and we assume the absolute differences as our systematic errors.
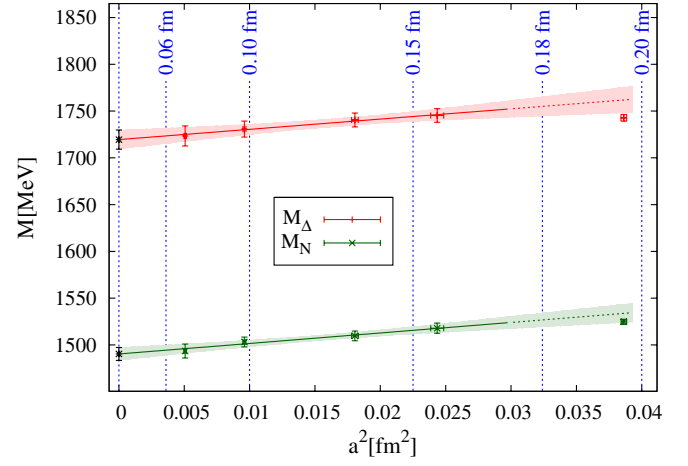
In a dedicated scaling test of light baryon masses, which included five lattice spacings with a total variation by almost a factor of 3, we have demonstrated that scaling violations associated with the use of our stout-link clover action in full QCD are small for these quantities. Indeed, we have shown that discretization errors on light baryon masses do not exceed 2% for lattice spacings up to 0.19 fm. Moreover, all our data for $a \lesssim 0.16$ fm seem to be in the scaling window. This is in line with the findings of [36] where a different approach to link smearing is taken.

In conclusion, we find that the combination of a tree-level Symanzik improved gauge action and a six-step stout-smeared clover fermion action with $c_{SW} = 1$ is well suited for precision calculations of physical observables. We expect that the same will be true of other actions with comparable improvements. We look forward to presenting results for phenomenological quantities with this action in forthcoming papers.

[1] M. Albanese *et al.* (APE), Phys. Lett. B **192**, 163 (1987).
[2] B. Sheikholeslami and R. Wohlert, Nucl. Phys. **B259**, 572 (1985).
[3] T. A. DeGrand, A. Hasenfratz, and T. G. Kovacs (MILC), arXiv:hep-lat/9807002.
[4] C. W. Bernard and T. A. DeGrand, Nucl. Phys. B, Proc. Suppl. **83**, 845 (2000).
[5] M. Stephenson, C. E. Detar, T. A. DeGrand, and A. Hasenfratz, Phys. Rev. D **63**, 034501 (2000).
[6] C. W. Bernard *et al.*, Nucl. Phys. B, Proc. Suppl. **94**, 346 (2001).
[7] J. M. Zanotti *et al.* (CSSM Lattice), Phys. Rev. D **65**, 074507 (2002).
[8] S. Capitani, S. Dürr, and C. Hoelbling, J. High Energy Phys. 11 (2006) 028.
[9] C. Morningstar and M. J. Peardon, Phys. Rev. D **69**, 054501 (2004).
[10] S. Duane, A. D. Kennedy, B. J. Pendleton, and D. Roweth, Phys. Lett. B **195**, 216 (1987).
[11] W. Kamleh, D. B. Leinweber, and A. G. Williams, Phys. Rev. D **70**, 014502 (2004).
[12] A. Hasenfratz, R. Hoffmann, and S. Schaefer, J. High Energy Phys. 05 (2007) 029.
[13] S. Dürr, arXiv:0709.4110.
[14] S. Schaefer, A. Hasenfratz, and R. Hoffmann, Proc. Sci., LAT2007 (2007) 132.
[15] R. Hoffmann, A. Hasenfratz, and S. Schaefer, Proc. Sci., LAT2007 (2007) 104.
[16] P. J. Moran and D. B. Leinweber, Phys. Rev. D **77**, 094501 (2008).
[17] M. Della Morte, R. Hoffmann, F. Knechtli, and U. Wolff (ALPHA), Comput. Phys. Commun. **165**, 49 (2005).
[18] S. Aoki *et al.* (JLQCD), Phys. Rev. D **72**, 054510 (2005).
[19] M. Lüscher and P. Weisz, Phys. Lett. **158B**, 250 (1985).
[20] R. Wohlert, DESY Report No. 87/069, 1987.
[21] R. Horsley, H. Perlt, A. Schiller, P. E. L. Rakow, and G. Schierholz, Proc. Sci., LAT2007 (2007) 250.
[22] M. Lüscher, S. Sint, R. Sommer, P. Weisz, and U. Wolff, Nucl. Phys. **B491**, 323 (1997).
[23] M. A. Clark, B. Joo, and A. D. Kennedy, Nucl. Phys. B, Proc. Suppl. **119**, 1015 (2003).
[24] M. A. Clark and A. D. Kennedy, Phys. Rev. Lett. **98**, 051601 (2007).
[25] T. A. DeGrand and P. Rossi, Comput. Phys. Commun. **60**, 211 (1990).
[26] A. Ali Khan *et al.* (QCDSF), Phys. Lett. B **564**, 235 (2003).
[27] C. Urbach, K. Jansen, A. Shindler, and U. Wenger, Comput. Phys. Commun. **174**, 87 (2006).
[28] J. C. Sexton and D. H. Weingarten, Nucl. Phys. **B380**, 665 (1992).
[29] M. Hasenbusch, Phys. Lett. B **519**, 177 (2001).
[30] T. Takaishi and P. de Forcrand, Phys. Rev. E **73**, 036706 (2006).
[31] L. Del Debbio, L. Giusti, M. Lüscher, R. Petronzio, and N. Tantalo, J. High Energy Phys. 02 (2006) 011.
[32] F. Farchioni *et al.*, Eur. Phys. J. C **39**, 421 (2005).
[33] F. Farchioni *et al.*, Eur. Phys. J. C **42**, 73 (2005).
[34] K. Jansen *et al.*, Proc. Sci., LAT2007 (2007) 036.
[35] S. Mignani and R. Rosa, Comput. Phys. Commun. **92**, 203 (1995)
[36] W. Kamleh, B. Lasscock, D. B. Leinweber, and A. G. Williams, Phys. Rev. D **77**, 014507 (2008).